Electrochemical behaviour of lithium–nickel oxides in molten carbonate

M.J. Escudero[a], T. Rodrigo[b], J. Soler[a], L. Daza[a,b,*]

[a]*Dpto. Combustibles Fósiles, CIEMAT, Av. Complutense 22, 28040 Madrid, Spain*
[b]*Instituto de Catálisis y Petroleoquímica, CSIC, Cantoblanco, 28049 Madrid, Spain*

Abstract

Impedance spectroscopy was used to investigate the stability and the catalytic activity of the lithium–nickel mixed oxides with high lithium content ($Li_xNi_{1-x}O$, $x = 0.30$–0.40) in a eutectic melt (Li:K) at 650 °C under a corrosive atmosphere (CO_2:O_2 4:1). The results were compared with a NiO reference cathode material. A modified transmission line model allowed to give a physical-meaning to the impedance spectra. All Li–Ni oxides showed similar catalytic activity and their impedance values were one order of magnitude lower than NiO. During the first 100 h of immersion, the samples showed structural changes due to the loss of lithium. Later on, the structure kept stable. The loss of lithium was confirmed by chemical analysis and X-ray diffraction (XRD). All Li–Ni oxide samples reduced the nickel dissolution in the eutectic in one order of magnitude in relation to NiO. In general, similar morphology was observed by scanning electron microscopy (SEM) for the fresh samples. After their immersion, the Li–Ni oxides did not show morphological change except for the sample with $x = 0.30$, for which a reduction of the particle size was observed. NiO presented an important morphological change due to its lithiation in situ.
© 2003 Elsevier Science B.V. All rights reserved.

Keywords: Lithium–nickel oxide; Molten carbonate fuel cell; MCFC; Cathode; Impedance spectroscopy; EIS

1. Introduction

The molten carbonate fuel cell (MCFC) has a great potential for high efficiency conversion of chemical energy to electricity energy. However, the life span of the MCFC remains insufficient for its commercial use. It is commonly recognised that the internal short-circuiting caused by the dissolution of NiO cathode is the most serious issue to tackle for long-term operation of the MCFC [1]. Doped lithium ferrate ($LiFeO_2$), lithium manganate (Li_2MnO_2) and lithium cobaltite ($LiCoO_2$) have been considered as candidates for cathode material. These oxides showed higher stability than NiO in MCFC conditions but their electrochemical performance is lower [2–6]. Recently, $LiCoO_2$-coated NiO and preoxised nickel–niobium surface alloy are being investigated as candidates for the MCFC cathode material [7–12].

The $Li_xNi_{1-x}O$ materials have being often studied for their applications as cathodic materials for lithium ion batteries [13–16] and as cathode materials for MCFC [17–22]. In this last case, Hatoh et al. showed that $Li_xNi_{1-x}O$ with high lithium content ($x > 0.2$) has a relatively lower rate of solubility than the $Li_xNi_{1-x}O$ cathode with a low lithium content ($0.02 < x < 0.05$) obtained with the in situ oxidised and lithiated NiO [18]. Other researchers have also proposed

high lithium content cathodes and studied the relationship between the lithium content and the porosity of the cathode. They showed that the porosity increased up to the composition 23 at.% Li^+, beyond which the porosity was nearly constant [19]. $Li_xNi_{1-x}O$, with high lithium content, can be obtained only by out-of-cell nickel oxidation and lithiation (by in-cell lithiation only low lithium content can be obtained). In our previous work, $Li_xNi_{1-x}O$ ($0.3 < x < 0.4$) prepared by ex situ lithiation showed higher stability in molten carbonate than NiO [23].

In this work, we have investigated the electrochemical behaviour of lithium–nickel mixed oxides with high lithium content. The stability and catalytic activity of lithiated samples were studied in an eutectic mixture of lithium and potassium (Li:K 62:38) at 650 °C by electrochemical impedance spectroscopy (EIS) as a function of immersion time under an oxidising gas mixture of CO_2:O_2 (4:1). The samples were characterised by X-ray diffraction (XRD), scanning electron microscopy (SEM) and inductive coupled plasma (ICP-AES) before and after their immersion to the carbonate melt. The NiO samples were tested using the same method and taken as reference.

2. Experimental

Nickel powder (99.9% Johnson & Matthey) with a particle size between (3–7 μm) and Li_2CO_3 (99%, Panreac)

* Corresponding author.
E-mail address: loreto.daza@fresno.csic.es (L. Daza).

were used as starting materials. Ni powder was added to a solution of Li_2CO_3 prepared in water (with a lithium atomic fraction in the range of 0.3–0.4). Remaining water was removed by rotating evaporator a 80 °C.

Three different samples were synthesised using a solid state reaction, containing a lithium atomic fraction of 0.4, 0.35 and 0.3 (denoted as $Li_{0.4}Ni_{0.6}O$, $Li_{0.35}Ni_{0.65}O$ and $Li_{0.3}Ni_{0.7}O$, respectively). A sample of metallic nickel powder was oxidised at 650 °C in air for 10 h to prepare the nickel oxide that was taken as reference. Precursor samples were pressed into pellets at 20 Tm cm^{-2} for 5 min. Then, the samples were calcined at 800 °C for 20 h.

The electrochemical experiments were performed in a test cell which was used in our previous study [24]. The cell was assembled with two identical electrodes to eliminate the influence of the counter electrode and to avoid the use of a reference electrode that is, by itself, a noise source [25]. The carbonate used was a mixture of 62% lithium carbonate and 38% potassium carbonate. About 75 g of the mixture was slowly heated to 650 °C with a ramp of 3 °C min^{-1}. Then, the electrodes were slowly put into the melt to avoid thermal shock and the cell temperature was kept constant. The cell impedance was measured as a function of immersion time from 1 to 200 h under an oxidising gas mixture $CO_2:O_2$ (4:1) to accelerate the dissolution of the cathode materials. The impedance spectra were collected by means of an AUTO-LAB system (PGSTAT30 and FRA2 module) from Eco Chemie B.V. The amplitude of the sinusoidal voltage signal for the impedance measurements was 5 mV. The measurements were performed at five points per frequency decade between 100 kHz and 100 µHz at the open circuit potential.

All samples prepared were characterised before and after the electrochemical tests by SEM using a Hitachi S-2500 and XRD using a SEIFERT 3000 P diffractometer with a Cu Kα radiation source. The Li and Ni contents of the samples were determined by ICP-AES (Jobin Yvon, JY-48/JY-38).
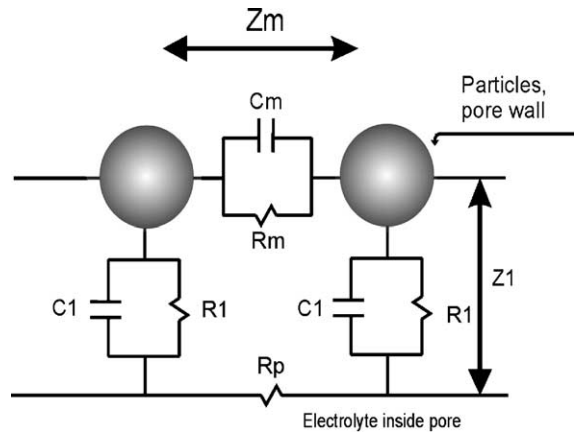

Fig. 1. Scheme of the transmission line used to the model the behaviour of Li–Ni oxides.

After the electrochemical tests, the concentration of nickel in the eutectic melt was also analysed by ICP-AES.

3. Fit procedure

The impedance data were analysed by using a modified transmission line model that was explained in our previous work [26]. The impedance function, Z, is given in Eq. (1):

$$Z(\omega) = R_e + Z_0(\omega) + Z_{TL}(\omega) \qquad (1)$$

where R_e accounts for the electrolyte resistance between both electrodes, $Z_0(\omega)$ the impedance associated to the inert volume of the electrode and the electrical contact, and Z_{TL} represents the impedance for the reacting volume, schematically illustrated in Fig. 1. The corresponding expression is Eq. (2):

$$Z_{TL}(\omega) = \frac{Z_m R_p L}{Z_m + R_p} + \frac{(Z_m^2 + R_p^2)\cosh(L\sqrt{\gamma}) + 2Z_m R_p}{(Z_m + R_p)\sqrt{\gamma}\sinh(L\sqrt{\gamma})} \qquad (2)$$
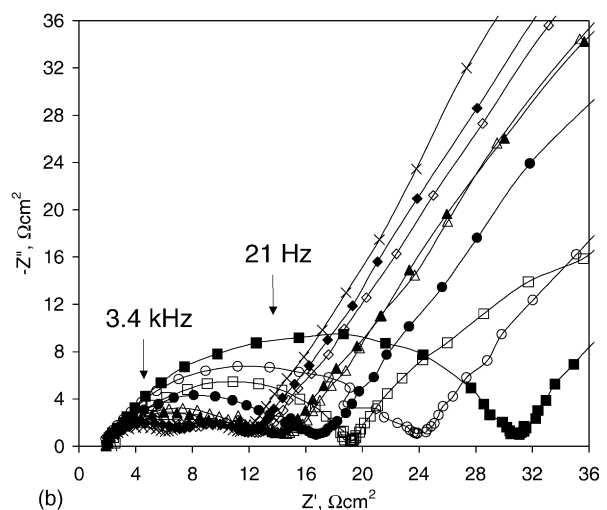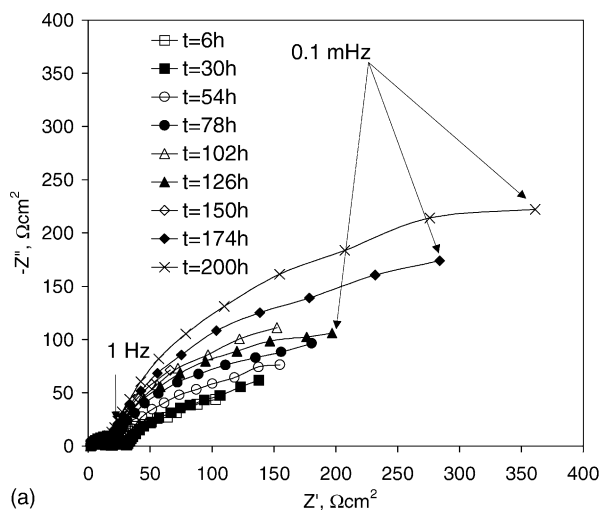

Fig. 2. Impedance spectra obtained for $Li_{0.4}Ni_{0.6}O$ as a function of immersion time: (a) low frequency region; (b) high frequency region.

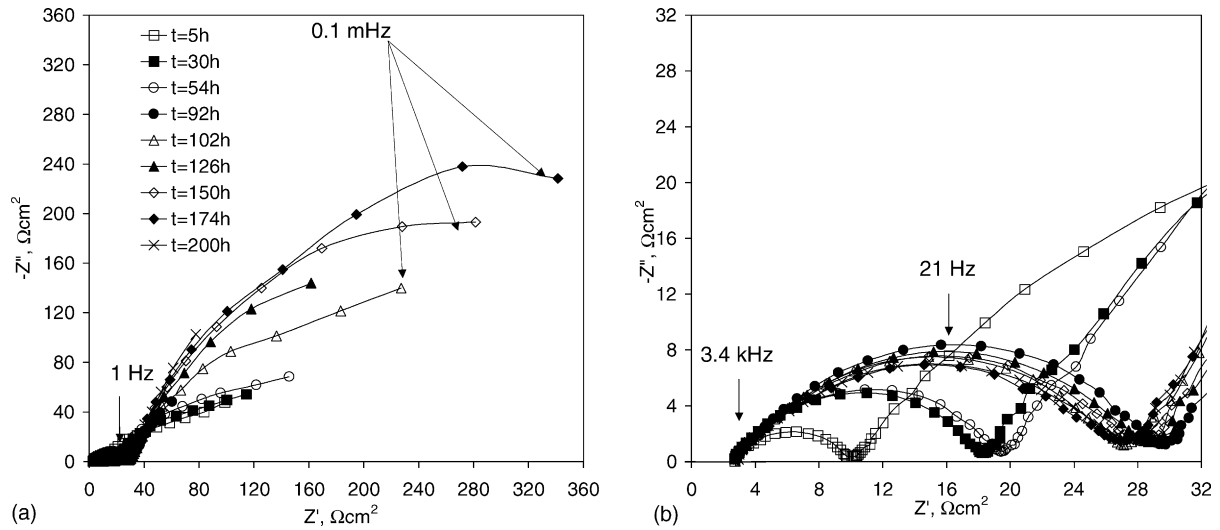Fig. 3. Impedance spectra obtained for $Li_{0.35}Ni_{0.65}O$ as a function of immersion time: (a) low frequency region; (b) high frequency region.
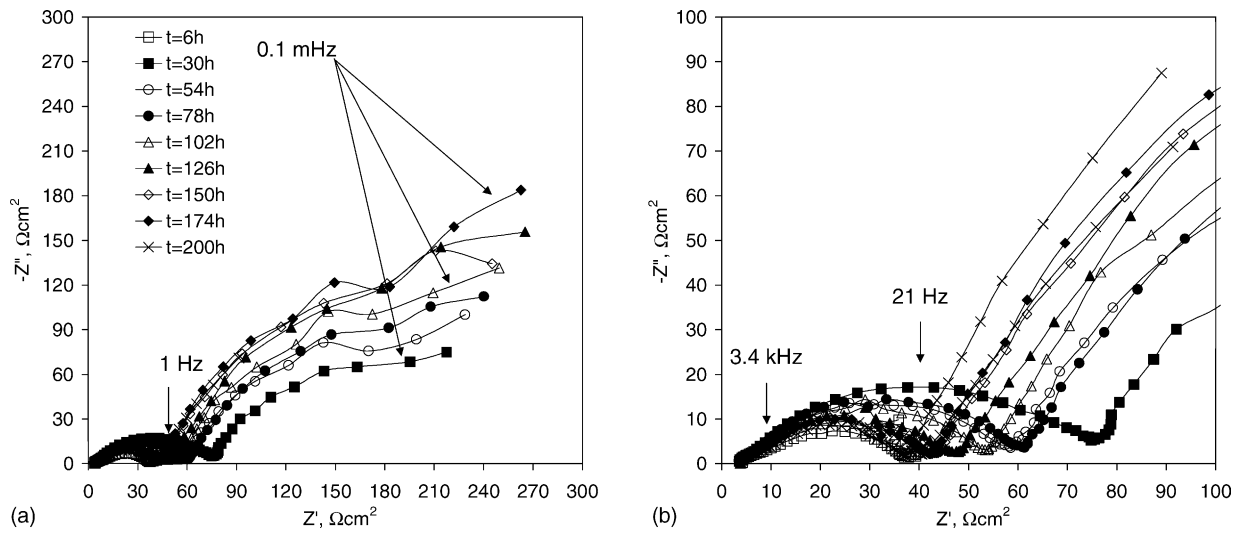

Fig. 4. Impedance spectra obtained for $Li_{0.3}Ni_{0.7}O$ as a function of immersion time: (a) low frequency region; (b) high frequency region.
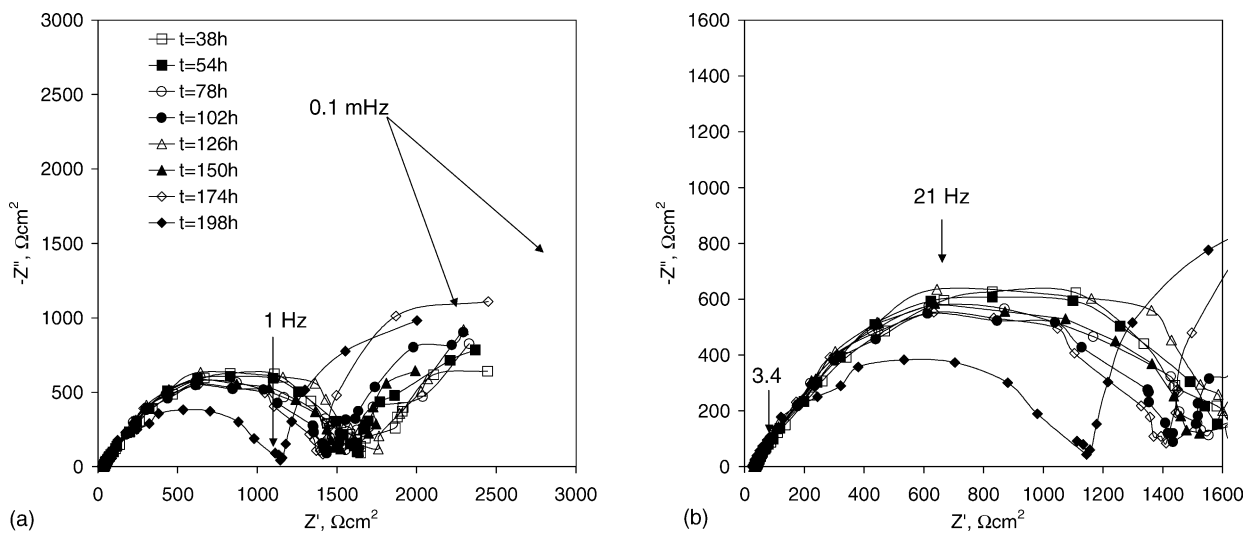

Fig. 5. Impedance spectra obtained for NiO as a function of immersion time: (a) low frequency region; (b) high frequency region.

where L is the thickness where the structural changes take place, $\gamma = (Z_m + R_p)/Z_1$ being Z_m the contact impedance along the transmission line and Z_1 the interfacial impedance corresponds to the double layer capacitance in parallel with the charge-transfer processes including the oxygen reduction, and R_p represents the electrolyte resistance along pores.

The intrinsic impedance, Z_0, the contact impedance, Z_m, and the interfacial impedance, Z_1, can be expressed by the following general equation for an RC parallel association (Eq. (3)):

$$Z_i(\omega) = \frac{R_i}{1 + (j\omega R_i C_i)^{\alpha_i}} \tag{3}$$

were the α_i parameter holds for Cole–Cole type dispersion of the $R_i C_i$ time constant.

The fitting procedure is based on the algorithm by Nelder and Mead [27] which uses the simplex method to find the minimum of a function. For the present case, the function to minimise, χ^2, is defined as

$$\chi^2 = \sum_{i=1}^{N} \left[\left(\frac{a_{ei} - a_{ci}}{0.01|Z_{ei}|} \right)^2 + \left(\frac{b_{ei} - b_{ci}}{0.01|Z_{ei}|} \right)^2 \right] \tag{4}$$

where N is the total number of scanned frequencies, a_{ei} and b_{ei} the real and imaginary parts of the experimental impedance Z_{ei}, $|Z_{ei}|$ the experimental impedance modulus at
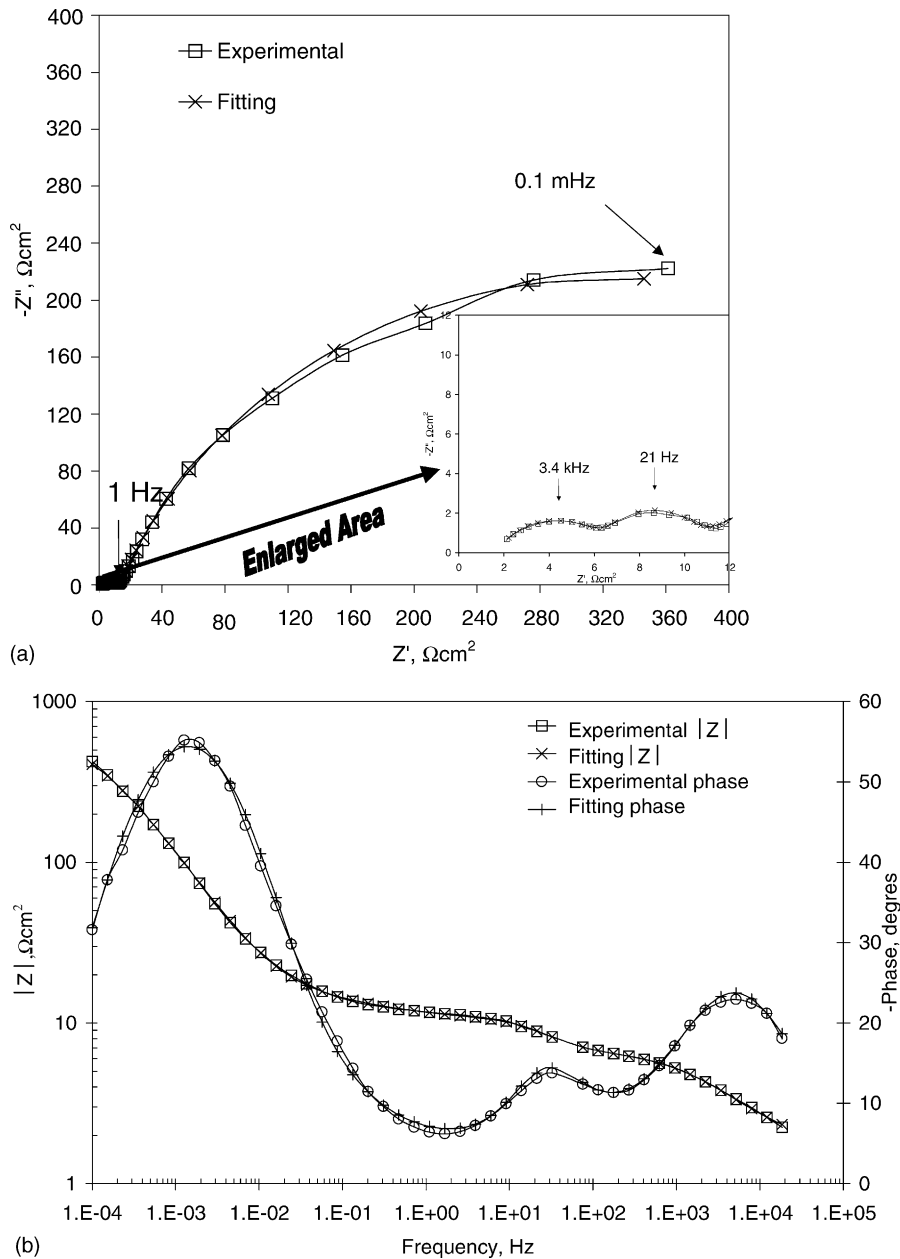

Fig. 6. Measured impedance spectra for $Li_{0.4}Ni_{0.6}O$ sample at 200 h with a gas composition $CO_2{:}O_2$ (4:1) compared to spectra calculated following Eq. (1): (a) Nyquist plot; (b) Bode plot.

frequency i, and a_{ci} and b_{ci} are the corresponding real and imaginary parts of the calculated impedance at frequency i. Eq. (4) implies that the experimental error is estimated as 1% of the impedance modulus and randomly distributed in the real and imaginary parts. Details of the fitting procedure are given in the publications [28,29].

4. Results and discussion

In Fig. 2, impedance diagrams are plotted at different times of immersion for the $Li_{0.4}Ni_{0.6}O$ sample an eutectic (Li:K 62:38) at 650 °C under an oxidising gas mixture of CO_2:O_2 (4:1). As can be observed from the Nyquist plots, two well-differentiated regions are present: below and over 1 Hz. In the high frequency region ($f > 1$ Hz) two arcs appeared; the second one showed variations during the first 100 h of immersion. The third arc in the low frequency region of the impedance spectra ($f < 1$ Hz) roughly increases on exposure times.

The impedance diagrams obtained for $Li_{0.35}Ni_{0.65}O$ and $Li_{0.3}Ni_{0.7}O$ are reported in Figs. 3 and 4, respectively. All diagrams showed the same features than $Li_{0.4}Ni_{0.6}O$. However, in the high region frequency ($f > 1$ Hz) it is more difficult to distinguish the two arcs. This may be due to a conjunction of the two arcs.
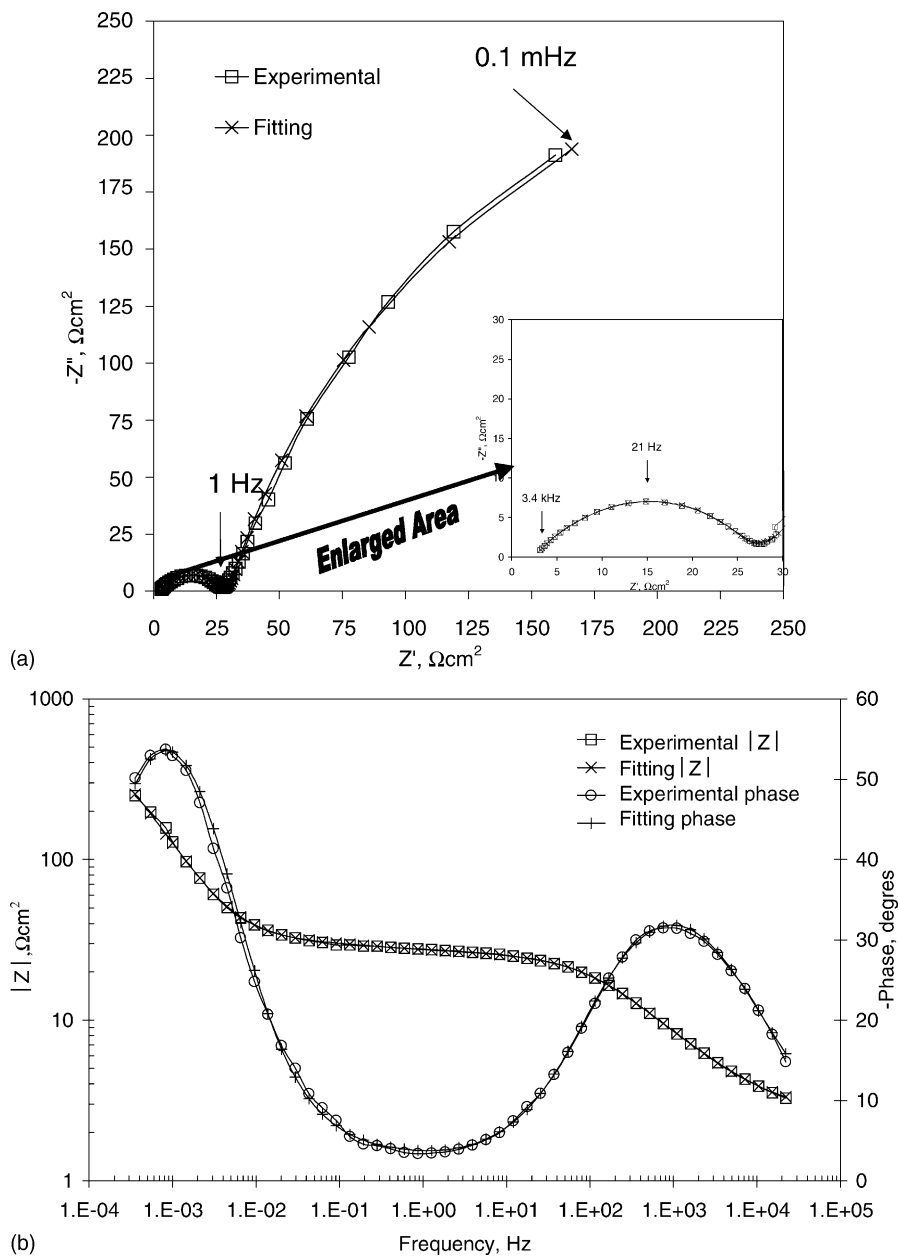

Fig. 7. Measured impedance spectra for $Li_{0.35}Ni_{0.65}O$ sample at 200 h with a gas composition CO_2:O_2 (4:1) compared to spectra calculated following Eq. (1): (a) Nyquist plot; (b) Bode plot.

Fig. 5 presents the impedance spectra for the nickel oxide taken as reference. The low frequency arc increases with the immersion time. In the high frequency region, the capacitive arc decreases at long exposure time. The reason could be the incorporation of lithium in its structure which enhances its electronic conductivity.

All impedance spectra were fitted to Eq. (1) which corresponds to the modified transmission line that considered the particle-to-particle contact and the processes of charge-transfer, in series with the impedance associated to the electrical contact and non-reactive volume. This modified transmission model allowed to give a physical interpretation of the three arcs observed in the

impedance diagrams. In the high frequency region, the first arc (at highest frequencies) associated with intrinsic impedance of the non-reacting volume, and the second one related with the impedance of particle-to-particle contact. During the first 100 h the variations observed in the second arc can be attributed to the structural changes in the reactive surface of the electrode due to the dissolution of lithium and the oxidation of nickel. After that, the structure seems to reach a stabilised state. The third arc, in the low frequency region corresponds to the charge-transfer processes associated with the catalytic activity (oxygen reduction). In all cases, the fits were very satisfactory in the whole frequency range. Four examples can be
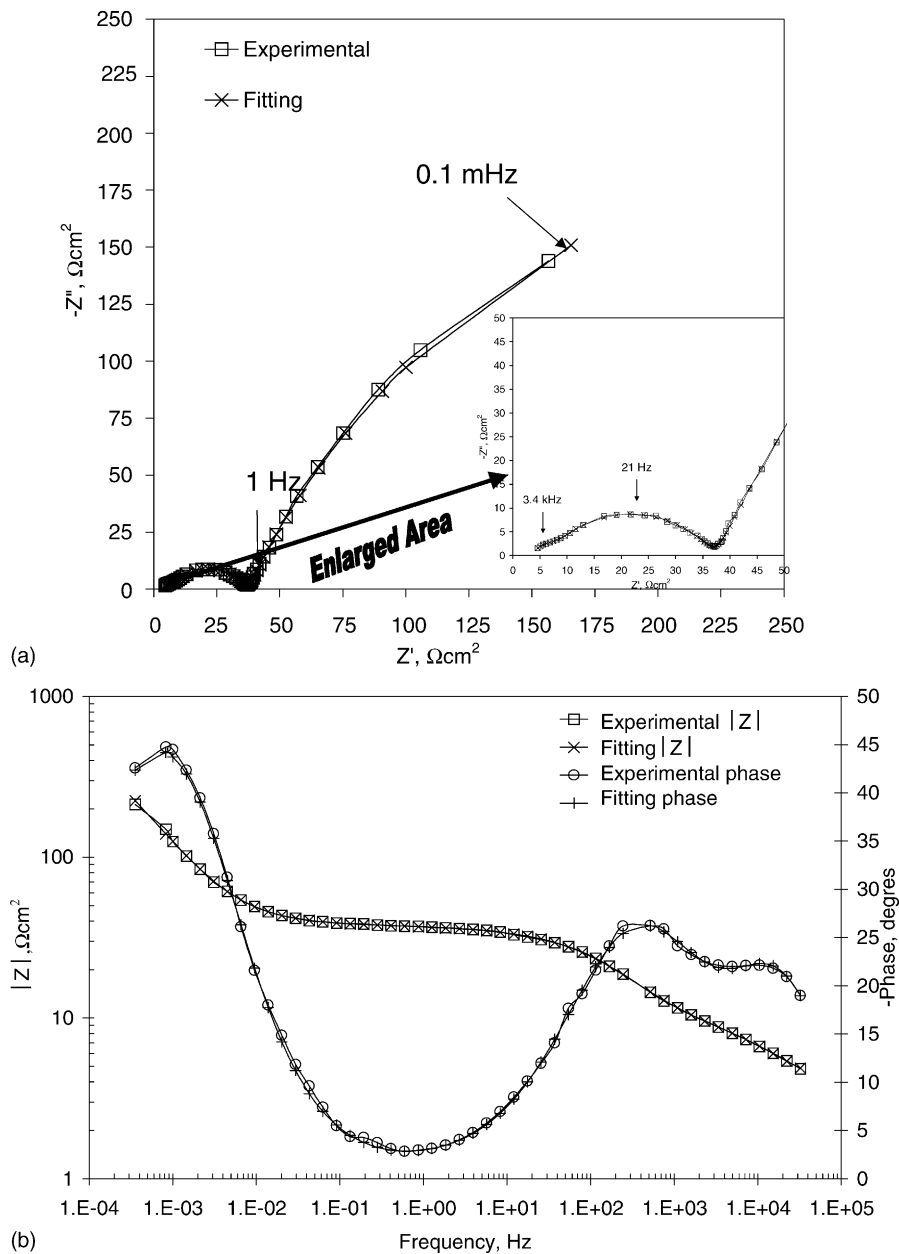
Fig. 8. Measured impedance spectra for $Li_{0.3}Ni_{0.7}O$ sample at 200 h with a gas composition $CO_2:O_2$ (4:1) compared to spectra calculated following Eq. (1): (a) Nyquist plot; (b) Bode plot.
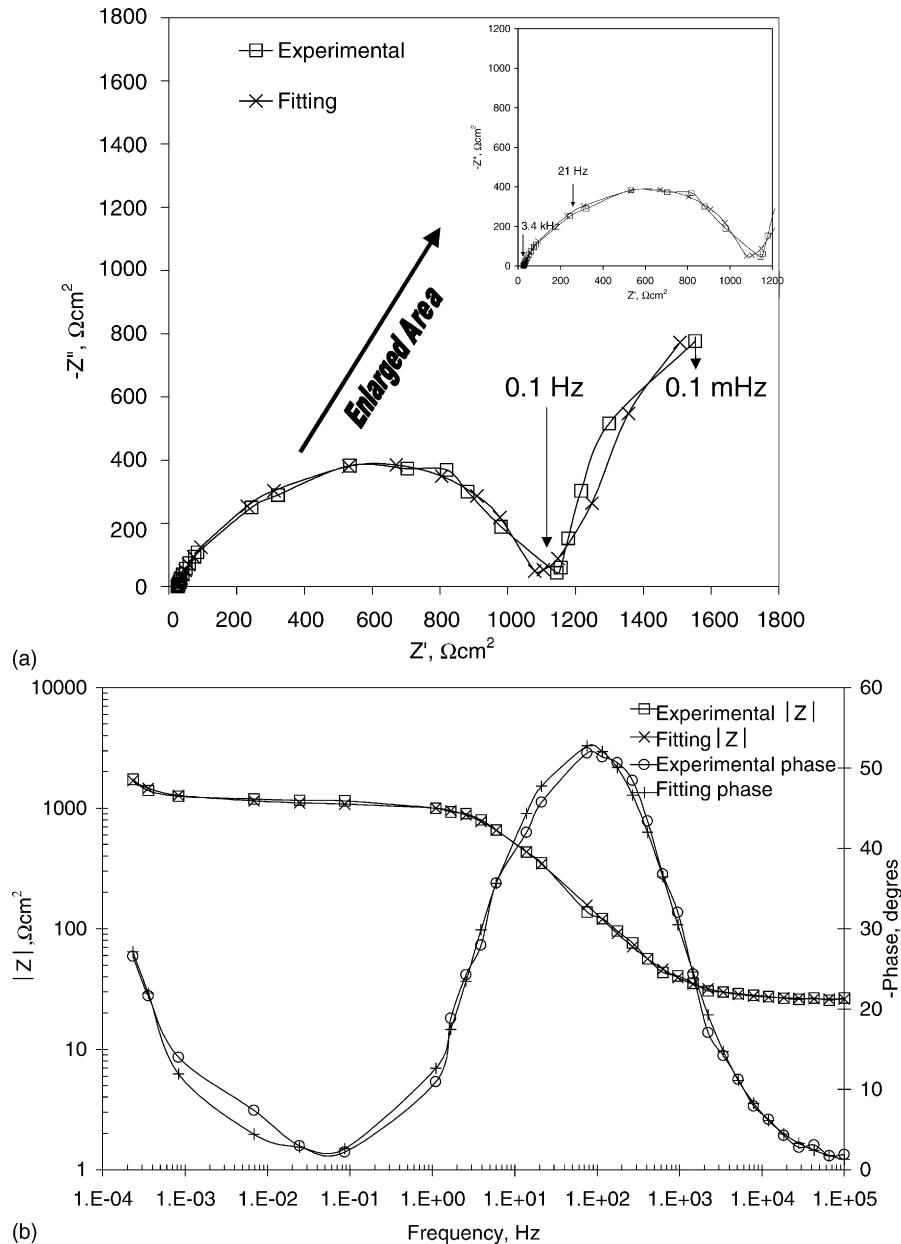
Fig. 9. Measured impedance spectra for NiO sample at 200 h with a gas composition $CO_2:O_2$ (4:1) compared to spectra calculated following Eq. (1): (a) Nyquist plot; (b) Bode plot.

seen in Figs. 6–9, where the experimental and fitted data are depicted in the Nyquist and Bode diagrams for all samples at 200 h of immersion. It is important to note that during the fitting procedure the pore length, L, was maintained constant and equal one fifth of the sample thickness (the transformed section at the end of the test, obtained by SEM observation of the cross-section).

Fig. 10 presents the evolution of the most significant model parameters with the immersion time for the Li–Ni mixed oxides. For $Li_{0.4}Ni_{0.6}O$, the structural changes are mainly related to the contact impedance between the nickel particles R_m increases and C_m decreases during the first 60 h of immersion (Fig. 10a). This could be due to the sample has reduced its conductivity by the loss of lithium that occurs

during the first hours of exposure. $Li_{0.35}Ni_{0.65}O$ and $Li_{0.3}Ni_{0.7}O$ showed similar behaviour in relation to R_m and C_m (Fig. 10b and c). The observed variation of the interfacial impedance (R_1 increases and C_1 decreases) suggests a loss of reactive surface with the immersion time. This could be due to a decrease of the active surface of each particle. Consequently, the charge-transfer process associated to the oxide oxidation, is less important with the exposure time. The resistance of the electrolyte inside the film, R_p, for $Li_{0.4}Ni_{0.6}O$ and $Li_{0.35}Ni_{0.65}O$ increases on immersion time that indicates pore blocking or pore length increasing. This last possibility correlates properly with R_0 variation, indicating a displacement of the electro-active front towards the electrode core. As can be seen in Fig. 10c,
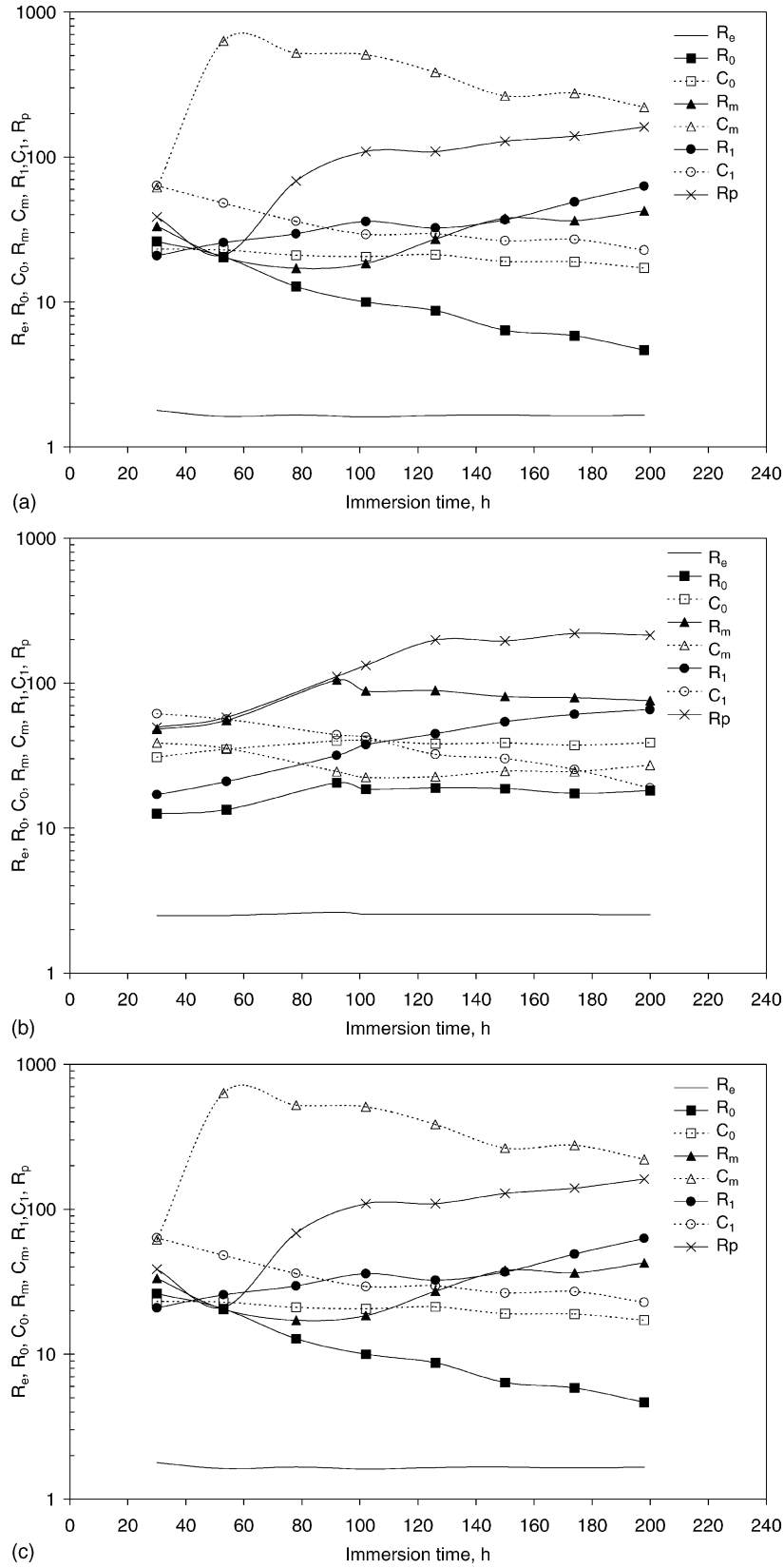
Fig. 10. Evolution of the model parameters on immersion time: (a) $Li_{0.4}Ni_{0.6}O$; (b) $Li_{0.35}Ni_{0.65}O$; (c) $Li_{0.3}Ni_{0.7}O$. The units on the y-axis are: R_e Ω cm^2, R_0 Ω cm^2, C_0 μF cm^{-2}, R_m Ω cm, C_m μF cm^{-1}, R_p Ω cm, R_1 Ω cm^3, C_m μF cm^{-3}.

$Li_{0.3}Ni_{0.7}O$ presents similar values for R_m and R_p that increase during the first 60 h and remains almost constant after 100 h. This can be attributed to a chemical change during the initial hours of exposure. The electrolyte resistance, R_e, is not influenced by the immersion time, that could indicate a low dissolution of nickel.

The influence of the lithium content for $Li_{0.4}Ni_{0.6}O$, $Li_{0.35}Ni_{0.65}O$, $Li_{0.3}Ni_{0.7}O$ and NiO at 200 h of the exposure in molten carbonate are depicted in Fig. 11. The experimental

and fitting impedance data were showed in Figs. 6–9 and the obtained values of the fit parameters are listed in Table 1. The values of fitting resistances are the same order of magnitude for the three Li–Ni oxides, except for R_m that is slight higher for $Li_{0.3}Ni_{0.7}O$. This is likely caused by a lower conductivity that increases the contact resistance, R_m, between particles. R_0, associated to the electrical contact and the inert volume is very sensible to the method of electrode preparation and whatever small variation in its manufacture
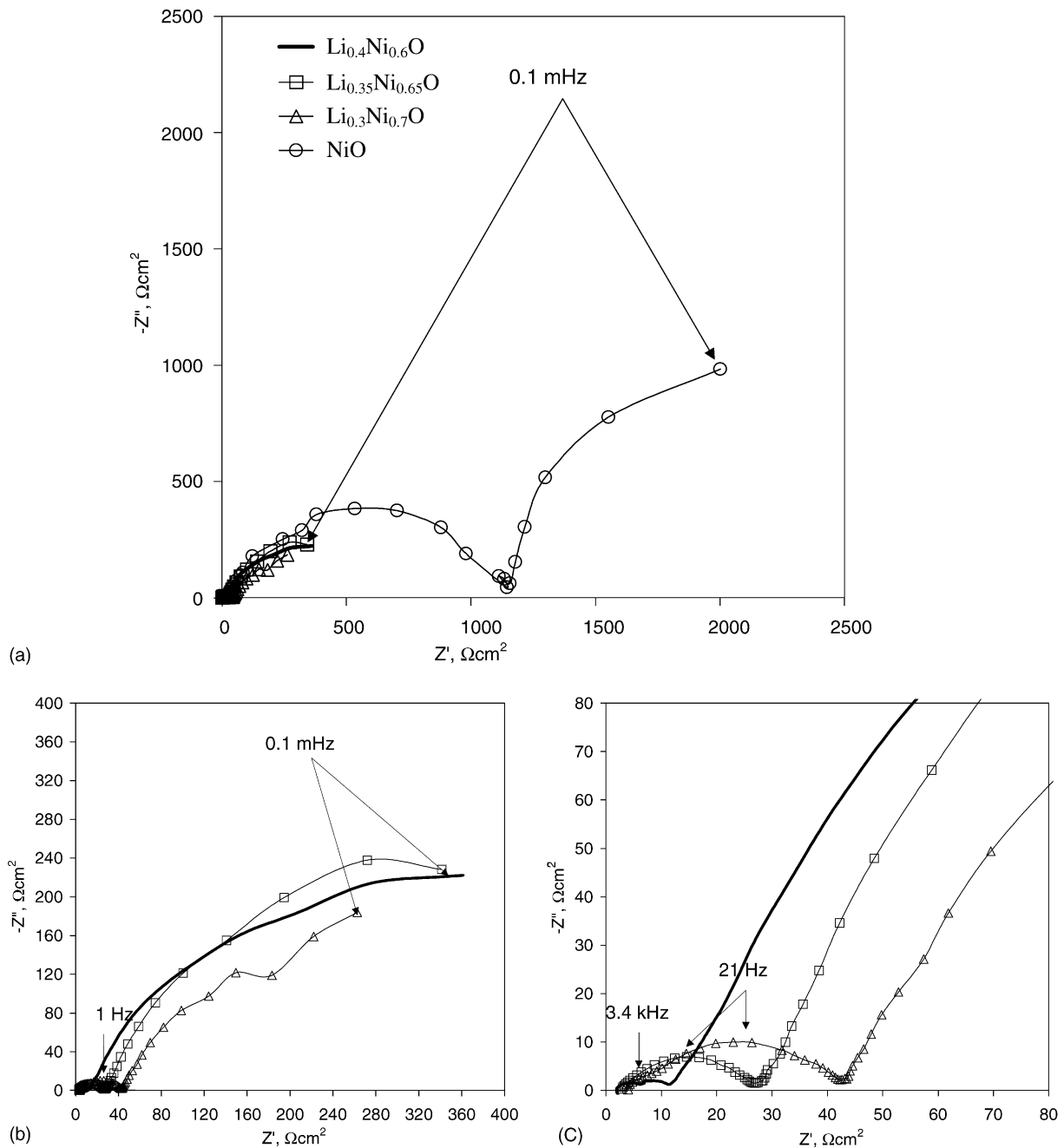

Fig. 11. Impedance spectra obtained at 200 h with a gas composition $CO_2:O_2$ (4:1): (a) $Li_{0.4}Ni_{0.6}O$, $Li_{0.35}Ni_{0.65}O$, $Li_{0.3}Ni_{0.7}O$ and NiO; (b) low frequency region for $Li_{0.4}Ni_{0.6}O$, $Li_{0.35}Ni_{0.65}O$ and $Li_{0.3}Ni_{0.7}O$; (c) high frequency region for $Li_{0.4}Ni_{0.6}O$, $Li_{035}Ni_{0.65}O$ and $Li_{0.3}Ni_{0.7}O$.

Table 1
Fitting parameters obtained using Eq. (1) for data given in Figs. 6–9

	$Li_{0.4}Ni_{0.6}O$ (Fig. 6)	$Li_{0.35}Ni_{0.65}O$ (Fig. 7)	$Li_{0.3}Ni_{0.7}O$ (Fig. 8)	NiO (Fig. 9)
R_e (Ω cm^2)	1.66	2.53	2.45	25.77
R_0 (Ω cm^2)	4.66	18.16	25.32	529.79
C_0 (F cm^{-2})	1.72E-5	3.88E-5	2.58E-5	2.49E-5
α_0	0.72	0.61	0.44	0.76
R_m (Ω cm^1)	42.62	75.60	228.24	9968.7
C_m (F cm^{-1})	2.21E-4	2.72E-5	1.53E-5	8.98E-5
α_m	0.97	0.88	0.95	0.98
R_1 (Ω cm^3)	62.93	65.72	52.15	237.06
C_1 (F cm^{-3})	22.78	18.89	21.26	7.86
α_1	0.76	0.84	0.80	1
R_p (Ω cm)	161.44	213.79	226.06	10260
L (mm)	1	1	1	1

could affect in its value. Furthermore, R_0 has less importance than R_m, due to its value is approximately 10 times lower for $Li_{0.4}Ni_{0.6}O$ and $Li_{0.35}Ni_{0.65}O$, and four times lower for $Li_{0.30}Ni_{0.7}O$. Similar capacitive values of C_0, C_m and C_1 were obtained for the three mixed oxides, we cannot distinguish the influence of lithium content due to it has the same order than the experimental error. The three Li–Ni mixed oxides show similar values capacitive arcs at low frequencies as can be seen in Fig. 11b and Table 1 (C_1 and R_1) This suggest a similar catalytic activity for the three samples.

The resistance values of NiO are one or two order of magnitude higher than the lithium–nickel oxides with high lithium content (Table 1 and Fig. 11a). This is likely caused by the lower conductivity of NiO compared to lithium–nickel samples [24]. Therefore, the use of these Li–Ni oxides
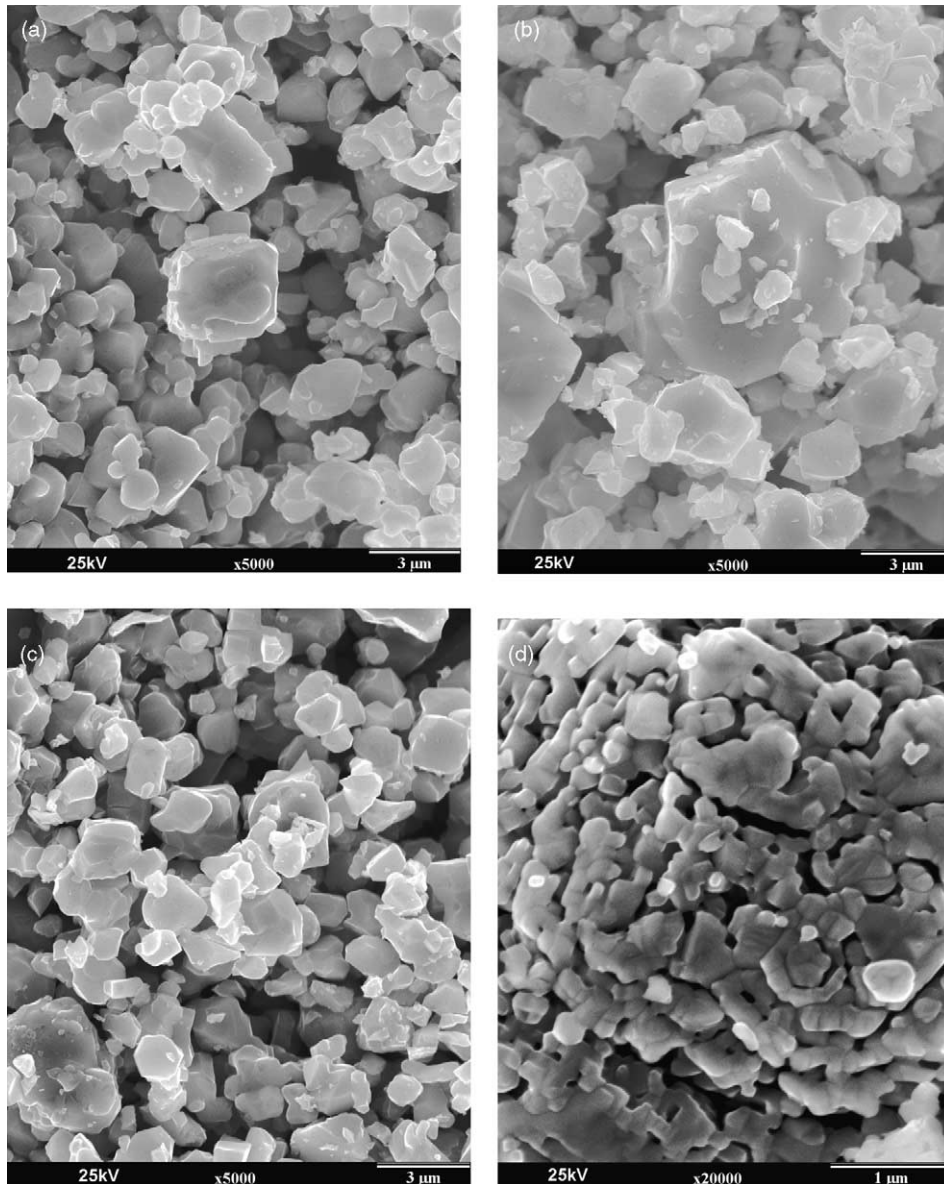

Fig. 12. SEM micrographs for the samples before testing: (a) $Li_{0.4}Ni_{0.6}O$; (b) $Li_{0.35}Ni_{0.65}O$; (c) $Li_{0.3}Ni_{0.7}O$; (d) NiO.

Table 2
Lithium atomic fraction of the samples before and after the electro-chemical tests and the nickel concentration in the eutectic melt

Sample	x_{Li} (before)	x_{Li} (after)	Ni (ppm)
$Li_{0.4}Ni_{0.6}O$	0.36	0.28	6.5
$Li_{0.35}Ni_{0.55}O$	0.31	0.26	3.2
$Li_{0.3}Ni_{0.7}O$	0.28	0.24	2.4
NiO	–	0.02	27.5

as cathode materials for MCFC will reduce the ohmic loss what could improve the cell performance.

$Li_{0.4}Ni_{0.6}O$ presented lower values of electrolyte resistance (R_e), inert resistance (R_0), contact resistance (R_m) and the electrolyte resistance along pores (R_p) and similar values of interface resistance (R_1) in relation to the other mixed

oxides. Therefore, $Li_{0.4}Ni_{0.6}O$ sample had the lowest impedance value and could be the best composition as alternative cathode material for MCFC.

Table 2 shows the lithium and nickel contents for the samples studied before and after the electrochemical test. After 200 h of immersion, the Li–Ni oxides suffered a loss of lithium from 22 to 14 at.%, but their lithium content (28–24 at.%) is higher than estimated by in situ lithiation nickel oxide (1–4 at.%) [30]. The nickel concentrations analysed in the eutectic for the Li–Ni oxides were between 6.5 and 2.7 ppm (µg Ni g^{-1} electrolyte). These values are one order of magnitude lower than measured by NiO (taken as reference) of 27.5 ppm.

The XRD diffraction patterns of the Li–Ni samples confirmed the loss of lithium measured by chemical analysis.
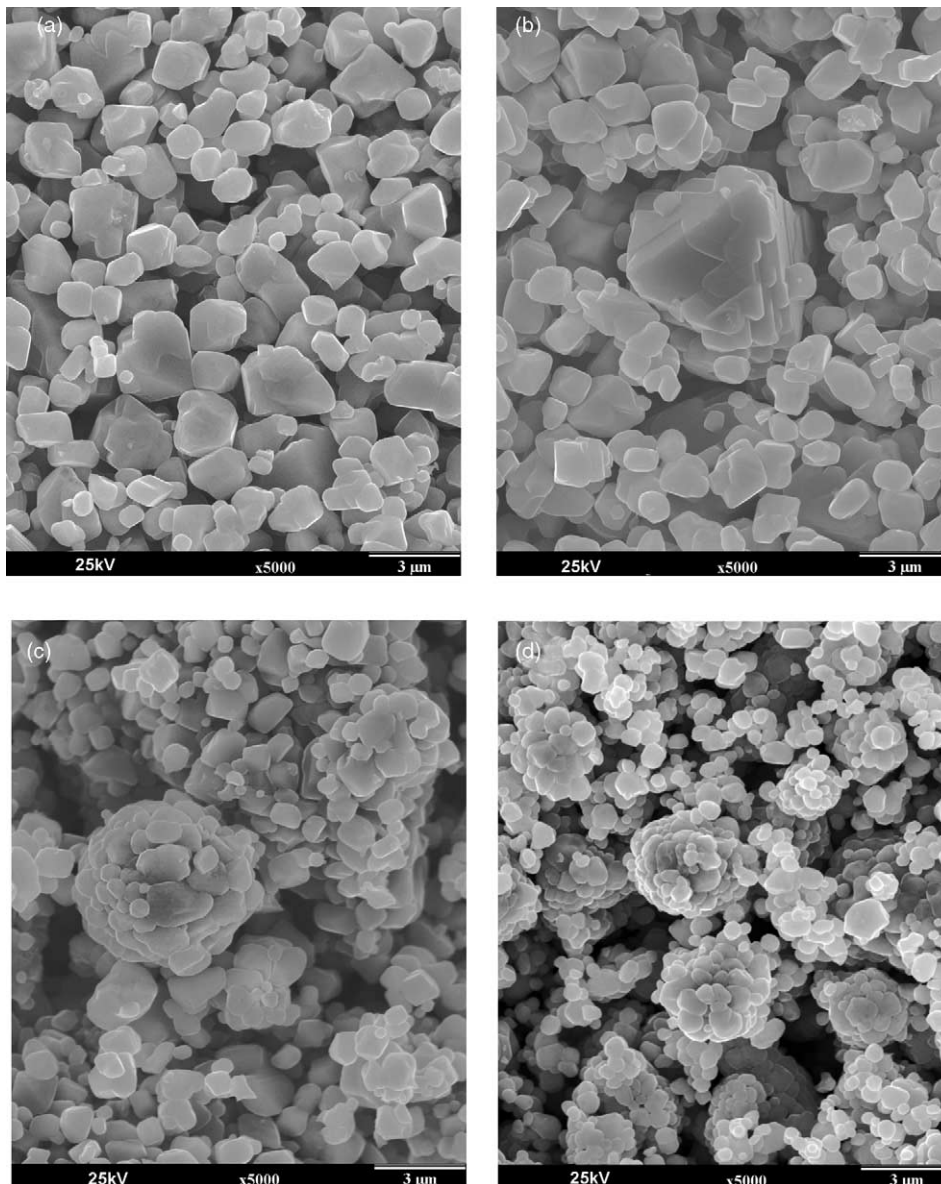

Fig. 13. SEM micrographs for the samples after testing: (a) $Li_{0.4}Ni_{0.6}O$; (b) $Li_{0.35}Ni_{0.65}O$; (c) $Li_{0.3}Ni_{0.7}O$; (d) NiO.

The scanning electron micrographs of the Li–Ni oxides and NiO before and after their immersion in the eutectic melt are shown in Figs. 12 and 13. Initially, the three novel materials showed a similar morphology and a particle size slight higher than the nickel oxide (Fig. 12). After their immersion in the carbonate electrolyte, the samples with higher lithium ($Li_{0.4}Ni_{0.6}O$ and $Li_{0.35}Ni_{0.65}O$) content showed slight morphological changes (Fig. 13a and b). While the sample with lower lithium content ($Li_{0.3}Ni_{0.7}O$) presented a reduction of the particle size due to the low concentration of lithium caused by its dissolution (Fig. 13c). On the contrary, the nickel oxide suffered important morphological changes due to the incorporation of lithium cation in its structure (Fig. 13d).

5. Conclusions

The impedance results show two well-differentiated regions in the Nyquist plots. In the high frequency region ($f > 1$ Hz) two arcs are present; the first one associated with the electrical contact and the impedance of inert volume, and the second one related to the particle to particle contact impedance. The third arc, in the low frequency region corresponds to the charger-transfer processes.

The impedance spectra of Li–Ni oxides presented modifications during the first 100 h of exposure that could be attributed to structural changes in the surface, mainly due to the diffusion of lithium ions from the surface of oxides to the carbonate melt. Similar catalytic activity was obtained by the $Li_xNi_{1-x}O$ with high lithium content, while the nickel oxide showed impedance values one order magnitude higher than the Li–Ni mixed oxides. This is likely due to its higher resistivity.

Chemical analysis of the Li–Ni mixed oxides showed a loss of lithium being their lithium concentration one order of magnitude higher than NiO lithiated in situ taken as reference. The dissolution of the nickel in the eutectic decreased also in one order of magnitude for $Li_xNi_{1-x}O$ with high lithium content.

XRD confirmed the loss of lithium measured by chemical analysis. Similar morphology was observed by SEM before and after their immersion for $Li_{0.4}Ni_{0.6}O$ and $Li_{0.35}Ni_{0.65}O$. While the $Li_{0.3}Ni_{0.7}O$ compound presented a reduction of the particle size due to the lower lithium content after its immersion. NiO showed important morphological change due to the incorporation of lithium in its structure.

$Li_{0.4}Ni_{0.6}O$ showed a structure stable after 100 h of exposure, the lowest impedance values and similar morphological after the test. Therefore, it could be a promising candidate as MCFC cathode material. Although it would be

necessary further investigation in single cell during long time operation.

References

[1] T. Kudo, Y. Hisamitsu, K. Kihara, M. Mohamedi, I. Uchida, J. Power Sources 104 (2002) 272.
[2] A.P. Brown, G.H. Kucera, M.F. Roche, in: Proceedings of the 2nd International Fuel Cell Conference, Japan, 5–18 February 1996, p. 125.
[3] L. Plomp, E.F. Sitters, C. Vessies, F.C. Eckes, J. Electrochem. Soc. 138 (1991) 629.
[4] B. Young Yang, K. Young Kim, Electrochim. Acta 44 (1999) 2227.
[5] S.T. Kuk, Y.S. Song, K. Kim, J. Power Sources 83 (1999) 50.
[6] T. Fukui, H. Okawa, T. Tsunooka, J. Power Sources 71 (1998) 239.
[7] B. Fang, H. Chen, J. Electroanal. Chem. 501 (2001) 128.
[8] B. Fang, C. Zhou, X. Liu, S. Duan, J. Appl. Electrochem. 31 (2000) 201.
[9] T. Fukui, S. Ohara, H. Okawa, T. Hotta, M. Naito, J. Power Sources 86 (2000) 340.
[10] J. Han, S.-G. Kim, S.P. Yoon, S.W. Nam, T.-H. Lim, S.-A. Hong, H.C. Lim, J. Power Sources 106 (2002) 153.
[11] D. Kim, M.-K. Kim, J.-T. Son, H.-G. Sim, J. Power Sources 108 (2002) 239.
[12] F.J. Pérez, D. Duday, M.P. Hierro, C. Gómez, M. Romero, M.T. Casais, J.A. Alonso, M.J. Martínez, L. Daza, J. Power Sources 72 (2000) 309.
[13] I.J. Pickering, P.D. Maddox, J.M. Thomas, Chem. Mater. 4 (1992) 1994.
[14] J.G. Chen, B.D. Vries, J.T. Lewandowski, R.H. Hall, Catal. Lett. 23 (1994) 25.
[15] K. Otsuka, K. Jinno, A. Morikawa, J. Catal. 100 (1986) 353.
[16] R.K. Ungar, X. Zhang, R.M. Labert, Appl. Catal. 42 (1988) L1.
[17] M.J. Escudero, X.R. Nóvoa, T. Rodrigo, L. Daza, J. Power Sources 106 (2002) 196.
[18] K. Hatoh, J. Nikura, E. Yasumoto, T. Gamo, Denki Kagaku 64 (1996) 825.
[19] E. Antolini, L. Giorgi, Ceramics Int. 24 (1998) 117.
[20] G. Xie, Y. Sakamura, K. Ema, Y. Ito, J. Power Sources 32 (1990) 125.
[21] G. Xie, Y. Sakamura, K. Ema, Y. Ito, J. Power Sources 32 (1990) 135.
[22] E. Antolini, J. Power Sources 40 (1992) 265.
[23] L. Daza, M.J. Escudero, E. Hontañón, C.M. Rangel, T. Rodrigo, M.T.Casais, M.J. Martínez, in: Proceedings of 2000 Fuel Cell Seminar, Portland, Oregon, USA, 30 October–2 November 2000, p. 732.
[24] M.J. Escudero, Ph.D. thesis, Universidad Autónoma de Madrid, Madrid, Spain, 2002.
[25] L. Giorgi, M. Carewska, S. Scaccia, E. Simoneti, E. Giacometti, R. Tulli, Int. J. Hydrogen Energy 21 (1996) 491.
[26] M.J. Escudero, X.R. Nóvoa, T. Rodrigo, L. Daza, J. Appl. Electrochem. 32 (2002) 929.
[27] J.A. Nelder, R. Mead, Comput. J. 7 (1985) 308.
[28] C.M. Abreu, M. Izquierdo, M. Keddam, X.R. Nóvoa, H. Takenouti, Electrochim. Acta 41 (1996) 2045.
[29] M. Keddam, H. Takenouti, X.R. Nóvoa, C. Andrade, C. Alonso, Chem. Conc. Res. 27 (1997) 1191.
[30] P. Tomczyk, M. Mosialek, J. Oblakowski, Electrochim. Acta 47 (2001) 945.